Synthesis, Structure, and Reactivity of (μ-Oxo)bis(μ-carboxylato)diiron(III) Complexes of a Dinucleating Dicarboxylate Ligand, Stable Models for Non-Heme Diiron Protein Cores

Stephen P. Watton, Axel Masschelein, Julius Rebek, Jr., and Stephen J. Lippard*

Contribution from the Department of Chemistry, Massachusetts Institute of Technology, Cambridge, Massachusetts 02139

Received January 14, 1994®

Abstract: Use of a pre-organized, cleft-shaped dicarboxylate ligand, *m*-xylenediamine-bis(Kemp's triacid)imide (XDK), in the self-assembly synthesis of (μ-oxo)bis(μ-carboxylato)diiron(III) complexes as models for the active site of non-heme diiron protein cores resulted in exclusive formation of dinuclear complexes. Reaction of H_2XDK with $Fe(NO_3)_3{\cdot}9H_2O$ in methanol solution afforded multigram quantities of a (μ-oxo)bis(μ-carboxylato)diiron(III) complex having six solvent ligands in the terminal positions. The geometry of this complex, $[Fe_2O(XDK)(CH_3OH)_5(H_2O)](NO_3)_2{\cdot}4H_2O$ (**1**$(NO_3)_2{\cdot}4H_2O$), was determined by X-ray crystallography, and Mössbauer spectroscopy demonstrated the persistence of its dinuclear structure in frozen methanol solution. Compound **1** reacted cleanly with N-donor ligands such as 2,2′-dipyridyl (bpy) to afford terminally substituted products, for example $[Fe_2O(XDK)(bpy)_2(CH_3OH)_2]^{2+}$ (**2**). The reactions were readily monitored by changes in the optical spectroscopic features of the complexes, and a stopped-flow kinetics analysis of the ligand exchange reaction revealed the second order rate constant k to be $(1.51 \pm 0.04) \times 10^3\ M^{-1}\ s^{-1}$. This value is quite similar to the rate constants for ligand substitution at the terminal site in hemerythrin. The substitution by two bpy ligands, one on each iron of the dinuclear center, proceeds at the same rate, except for a statistical factor of 2 favoring binding of the first equivalent, so that $k = k_2 = 0.5k_1$. Various solid products were obtained from this reaction, $[Fe_2O(XDK)(bpy)_2XY]^{n+}$, depending upon the isolation procedure used. Crystallization from a methanol/diethyl ether mixture gave the unsymmetrical complex **3** (X = CH_3OH, Y = NO_3^-, n = 1); recrystallization from CH_2Cl_2/toluene gave the symmetrical *anti*-**4** (X = Y = NO_3^-, n = 0); and recrystallization from acetonitrile afforded *syn*-**4** (X = Y = NO_3^-, n = 0), the X-ray structure of which is reported. Reaction of **1**$(NO_3)_2$ with 1-methylimidazole (1-MeIm) in methanol solution resulted in successive replacement of each of the terminal solvent ligands, affording $[Fe_2O(XDK)(1\text{-MeIm})_6]^{2+}$ (**5**). Formation of this complex was monitored spectroscopically with the use of UV/visible and resonance Raman spectroscopy, and its solid state structure was determined by X-ray crystallographic analysis of the tetraphenylborate salt.

Introduction

The occurrence of carboxylate-bridged diiron centers at the active sites of non-heme iron proteins such as hemerythrin (Hr), ribonucleotide reductase (RR), purple acid phosphatase (PAP), and methane monooxygenase (MMO) has stimulated extensive study of low molecular weight models for their dimetallic cores.[1-5] Although a large number of structurally and spectroscopically relevant model complexes for both the reduced and oxidized forms of the protein active sites now exist, the biological activities have not yet been effectively reproduced. One difficulty associated with achieving biomimetic reactions with non-heme iron-containing model complexes stems from rapid substitution kinetics at the metal ions, which afford access to multiple binding modes and a variety of oligomeric products. This situation contrasts with the behavior of the protein-bound non-heme iron centers, where the three-dimensional folding of the polypeptide chain imposes thermodynamic and kinetic restrictions on the active site chemistry. The result is specific and controlled reactivity.

In order to provide better control over the reactivity of carboxylate-bridged diiron model complexes, with the ultimate aim of reproducing the functions of metalloproteins and enzymes containing these units, we have been exploring the extent to which the principles of molecular recognition in organic chemistry might be applied to bioinorganic modeling studies. Specifically, we have employed the cleft-shaped dicarboxylate ligand xylenediamine-bis(Kemp's triacid)imide,[6,7] hereafter XDK, to assemble

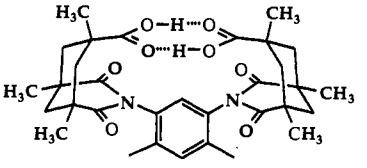

$XDKH_2$

a dinuclear $\{Fe_2O(XDK)\}^{2+}$ core structure having six labile solvento ligands in the terminal positions, $[Fe_2O(XDK)(CH_3OH)_5(H_2O)]^{2+}$ (**1**). This remarkable complex is resistant to oligomerization, existing entirely as the dinuclear species in solution. Moreover, compound **1** readily converts to a variety of (oxo)bis(carboxylato)-bridged dinuclear Fe(III) derivatives, and in this respect it is superior to our previous attempt to use a dinucleating dicarboxylate ligand to stabilize the $\{Fe_2O(O_2CR)_2\}^{2+}$ core.[8] In the present article we describe the synthesis,

* Abstract published in *Advance ACS Abstracts*, May 1, 1994.

(1) Lippard, S. J. *Angew. Chem., Int. Ed. Engl.* **1988**, *27*, 344–361.
(2) Sanders-Loehr, J.; Wheeler, W. D.; Shiemke, A. K.; Averill, B. A.; Loehr, T. M. *J. Am. Chem. Soc.* **1989**, *111*, 8084–8093.
(3) Kurtz, D. M., Jr. *Chem. Rev.* **1990**, *90*, 585–606.
(4) Vincent, J. B.; Olivier-Lilley, G. L.; Averill, B. A. *Chem. Rev.* **1990**, *90*, 1447–1467.
(5) Que, L., Jr.; True, A. E. *Prog. Inorg. Chem.* **1990**, *38*, 97–200.
(6) Rebek, J., Jr.; Marshall, L.; Wolak, R.; Parris, K.; Killoran, M.; Askew, B.; Nemeth, D.; Islam, N. *J. Am. Chem. Soc.* **1985**, *107*, 7476–7481.
(7) Marshall, L.; Parris, K.; Rebek, J., Jr.; Luis, S. V.; Burguete, M. I. *J. Am. Chem. Soc.* **1988**, *110*, 5192–5193.
(8) Beer, R. H.; Tolman, W. B.; Bott, S. G.; Lippard, S. J. *Inorg. Chem.* **1991**, *30*, 2082–2092.

0002-7863/94/1516-5196$04.50/0

characterization, and terminal ligand substitution reactions of **1**, the last of which should be of value for understanding ligand exchange processes taking place during turnover in the enzymatic systems. The utility of **1** in preparing a model for the dinuclear iron center and nearby tyrosyl radical in the RR R2 protein was previously communicated.[9] Dinuclear iron(II) complexes of XDK have been independently investigated, but in the context of capping rather than skeletal ligation.[10]

Experimental Section

Materials and Methods. H_2XDK was prepared as described previously,[6,7] except that the 2,4-diamino-*m*-xylene starting material was obtained by an alternative, more convenient procedure, involving nitration of *m*-xylene followed by fractional crystallization and catalytic hydrogenation of the 2,5-dinitroxylene product. The complex $[Fe(bpy)(NO_3)_2]_2O$ was also prepared by a literature procedure.[11] All reagents were purchased from commercial sources and used as received unless otherwise noted.

Preparation of Compounds. $[Fe_2O(XDK)(CH_3OH)_5(H_2O)](NO_3)_2 \cdot 4H_2O$, $\mathbf{1}(NO_3)_2 \cdot 4H_2O$. This complex was prepared by treating a suspension of H_2XDK (5.0 g, 8.6 mmol) in methanol (100 mL) with $Fe(NO_3)_3 \cdot 9H_2O$ (6.87 g, 17 mmol) to give a deep green solution. Diethyl ether was added to bring the volume to 250 mL, the mixture was filtered, and the filtrate was cooled to −20 °C overnight. The complex was obtained as green blocks which were collected and dried in air. Yield 6.8 g, 73%. Anal. Calcd for $C_{37}H_{68}N_4O_{25}Fe_2$: C, 41.12; H, 6.34; N, 5.18. Found: C, 41.43; H, 5.74; N, 5.63. FTIR (KBr pellet): 3400 (br), 3196 (br), 2969, 1733, 1671, 1543, 1470, 1415, 1372, 1295, 1202, 1095, 1021, 961, 885, 846, 773, 634, 519 cm^{-1}. UV/vis (CH_3OH), λ_{max}, nm (ε, Fe^{-1}, M^{-1} cm^{-1}): 358 (1656), 474 (157), 616 (57). Raman (CH_3OH): ν_{sym}(Fe–O–Fe) = 532 cm^{-1}. Mössbauer (solid state): Site 1, δ = 0.55 mm s^{-1}, ΔE_Q = 1.67 mm s^{-1}. Site 2. δ = 0.56 mm s^{-1}, ΔE_Q = 2.06 mm s^{-1}; (CH_3OH, frozen solution): δ = 0.56 mm s^{-1}, ΔE_Q = 1.87 mm s^{-1}.

$[Fe_2O(XDK)(bpy)_2(CH_3OH)(NO_3)](NO_3)$, $\mathbf{3}(NO_3)$. A portion of $[Fe_2O(XDK)(CH_3OH)_5(H_2O)](NO_3)_2$ (0.250 g, 0.227 mmol) was stirred in 1 mL of methanol to give a deep green solution. Solid 2,2′-dipyridine (0.071 g, 0.454 mmol) was added and the resulting brown solution was stirred for 5 min and then filtered. Vapor diffusion of ether into this solution at room temperature afforded the product as brown blocks. Yield, 0.285 g (96%). Anal. Calcd for $C_{53}H_{58}N_8O_{16}Fe_2$: C, 54.19; H, 4.98; N, 9.54. Found: C, 53.83; H, 5.02; N, 9.54. FAB-MS (3-NBA matrix): *m/e* 1080 ($M^+ - CH_3OH$), 1018 (1080 − NO_3), 924 (1080 − bpy), 862 (1018 − bpy). FTIR (KBr pellet): 3419 (br), 3264 (br, sh), 2978, 2920, 1731, 1686, 1605, 1549, 1453, 1368, 1325, 1288, 1190, 1104, 1029, 964, 892, 848, 774, 733, 659, 634 cm^{-1}. UV/vis (CH_3OH), λ_{max}, nm (ε, Fe^{-1}, M^{-1} cm^{-1}): 330 sh (4145), 364 sh (2702), 461 (439), 490 (440), 528 sh (111), 694 (70).

anti*-$[Fe_2O(XDK)(bpy)_2(NO_3)_2]$, *anti*-4.** ***Method 1. The compounds H_2XDK (0.100 g, 172 μmol) and $[Fe(bpy)(NO_3)_2]_2O$ (0.118 g, 172 μmol) were stirred in 10 mL of methanol, and Et_3N (46 μL, 350 μmol) was added. The resulting deep green-brown solution was filtered to remove a small amount of red material, then ether (50 mL) was added to precipitate the product. The pale green-brown solid was collected and dried (160 mg, 81%). The complex was recrystallized from CH_2Cl_2/toluene as large dark green blocks. The yield of crystallized material was 0.100 g (50% based on H_2XDK). Anal. Calcd for $C_{52}H_{54}N_8O_{15}Fe_2$: C, 54.66; H, 4.76; N, 9.81. Found (mean of two samples): C, 54.69 ± 0.90; H, 4.72 ± 0.05; N, 9.65 ± 0.04. FAB-MS (NBA matrix): *m/e* 1080 ($M^+ - NO_3$), 1018 ($M^+ - 2NO_3$), 924 (1080 − bpy), 862 (1018 − bpy). FTIR (KBr pellet): 3417, 2978, 2934, 1727, 1696, 1553, 1461, 1360, 1190, 770, 734 cm^{-1}. UV/vis (CH_2Cl_2), λ_{max}, nm (ε, Fe^{-1}, M^{-1} cm^{-1}): 330 (5837), 365 (3337), 464 (448), 484 (426), 686 (79). Raman ($CHCl_3$): ν_{sym}(Fe–O–Fe) 532 cm^{-1}.

Method 2. Compound $\mathbf{3}(NO_3)$ (0.100 g, 85 μmol) was recrystallized from CH_2Cl_2/toluene to give 0.07 g (75%) of green crystals, identical by IR spectroscopy with the product prepared by Method 1.

***syn*-$[Fe_2O(XDK)(bpy)_2(NO_3)_2]$, *syn*-4.** The *syn* isomer of **4** was prepared by using the methods described for the *anti* isomer (above), except that acetonitrile was employed in the recrystallizations, affording the product as green blocks.

Method 1. Reaction of 0.100 g (172 μmol) of H_2XDK, 0.118 mg (172 μmol) of $[Fe(bpy)(NO_3)_2]_2O$, and 46 μL of $(C_2H_5)_3N$ in 10 mL of CH_3OH afforded 0.100 g (51%) after recrystallization from 10 mL of acetonitrile.

Method 2. A 0.085-g (0.227 mmol) portion of $\mathbf{3}(NO_3)$ was recrystallized from 8 mL of acetonitrile to afford 0.050 g (60.4%) of *syn*-**4**. Anal. Calcd for $C_{52}H_{54}N_8O_{15}Fe_2$: C, 54.66; H, 4.76; N, 9.81. Found: C, 54.15; H, 4.75; N, 10.18. FTIR (thin film on KBr plate): 2962, 2926, 1732, 1690, 1654, 1541, 1405, 1356, 1230, 1197, 1023, 968, 835, 768, 736, 695 cm^{-1}. UV/vis (CH_3CN) λ_{max}, nm (ε, Fe^{-1}, M^{-1} cm^{-1}): 332 sh (3707), 366 sh (2375), 482 (432), 528 sh (143), 684 (100).

$[Fe_2O(XDK)(1\text{-MeIm})_6](BPh_4)_2 \cdot CHCl_3$, $\mathbf{5}(BPh_4)_2 \cdot CHCl_3$. The complex was prepared by treatment of $\mathbf{1}(NO_3)_2$ (0.2 g, 0.19 mmol) with an excess of 1-MeIm (0.87 mL, 57 equiv) in methanol (2 mL) to give a deep green-brown solution. A solution of $NaBPh_4$ (0.25 g, 0.73 mmol) in methanol (2 mL) was added, affording a pale green precipitate, which was collected by filtration and dried (yield 0.34 g, 96%). The complex was recrystallized by vapor diffusion of hexane into a concentrated chloroform solution. Anal. Calcd for $C_{104}H_{114}N_{14}O_9Fe_2B_2$: C, 67.98; H, 6.25; N, 10.67. Found: C, 67.43; H, 6.29; N, 10.72. FTIR (KBr pellet) 3134, 3051, 2978, 2921, 1729, 1658, 1540, 1469, 1424, 1368, 1275, 1226, 1191, 1099, 1026, 949, 849, 736, 701, 662, 614, 501 cm^{-1}. UV/vis ($CHCl_3$) λ_{max}, nm (ε, Fe^{-1}, M^{-1} cm^{-1}): 330 sh (2147), 364 sh (1796), 480 (271), 680 (49). Raman (CH_3OH): ν_{sym}(Fe–O–Fe) 505 cm^{-1}.

X-ray Crystallography. Data collection and reduction, including corrections for Lorentz, polarization, and absorption effects, were performed by using general procedures previously described.[12] No appreciable decay was observed for any of the compounds, as judged by periodic monitoring of the intensities of three standard reflections. Initial iron positions were obtained by using the direct methods programs MITHRIL and SHELXS-86[13] for **1**, **4**, and **5**. The remaining heavy atoms were located with DIRDIF phase refinements and difference Fourier maps.[14] The TEXSAN package of programs was used to refine the structures.[15] A summary of data collection parameters for complexes **1**, **4**, and **5** is given in Table 1.

$[Fe_2O(XDK)(CH_3OH)_5(H_2O)](NO_3)_2 \cdot 4H_2O$, $\mathbf{1}(NO_3)_2 \cdot 4H_2O$. The crystal used in the X-ray diffraction study, obtained directly from the synthetic procedure described above (dimensions 0.4 × 0.4 × 0.5 mm), was mounted in Paratone N on the end of a quartz fiber and frozen at 195 ± 1 K. Data collection and structure solution were performed as described above. The positions of all atoms were refined anisotropically, with the exception of the lattice solvents, which were refined with isotropic thermal parameters. The hydrogen atoms bound to O1, O2, and O3 were located from difference Fourier maps, assigned isotropic thermal parameters, and refined. The carbon-bound hydrogen atoms were placed at calculated positions in the final refinement cycles. The hydrogen atom bound to O4 was not located. The largest peak in the final difference Fourier map was approximately 0.52 $e^-/Å^3$, located in the vicinity of the lattice solvents.

***syn*-$[Fe_2O(XDK)(bpy)_2(NO_3)_2] \cdot 3CH_3CN$, *syn*-4·3CH₃CN.** The crystal used in the X-ray study was obtained by recrystallization at room temperature, as described above (Method 1). A brown-green block (dimensions 0.1 × 0.1 × 0.15 mm) was mounted on a glass fiber using Paratone N oil. Data were collected at 195 ± 1 K with ω–2θ scans. Psi-scans for four independent reflections indicated that no correction was needed for absorption effects, the relative intensities varying from 0.95 to 1.00. All non-hydrogen atoms were refined anisotropically, except for those of the lattice acetonitrile molecules, which were refined using isotropic temperature factors. Hydrogen atoms were included in the final cycles of least-squares refinement at calculated positions. The largest electron density peak in the final difference Fourier map corresponded to 0.7 $e^-/Å^3$, located near a lattice acetonitrile molecule.

$[Fe_2O(XDK)(1\text{-MeIm})_6](BPh_4)_2 \cdot CHCl_3$, $\mathbf{5}(BPh_4)_2 \cdot CHCl_3$. The crystal used in the X-ray study was grown by vapor diffusion of hexane into a

(9) Goldberg, D. P.; Watton, S. P.; Masschelein, A.; Wimmer, L.; Lippard, S. J. *J. Am. Chem. Soc.* **1993**, *115*, 5346–5347.
(10) Hagen, K. S.; Lachicotte, R.; Kitaygorodskiy, A.; Elbouadili, A. *Angew. Chem., Int. Ed. Engl.* **1993**, *32*, 1321–1324.
(11) Taft, K. L.; Masschelein, A.; Liu, S.; Lippard, S. J.; Garfinkel-Shweky, D.; Bino, A. *Inorg. Chim. Acta* **1992**, *198–200*, 627–631.
(12) Carnahan, E. M.; Rardin, R. L.; Bott, S. G.; Lippard, S. J. *Inorg. Chem.* **1992**, *31*, 5193–5201.
(13) Sheldrick, G. M. In *Crystallographic Computing 3*; Sheldrick, G. M., Krüger, C., Goddard, R., Eds.; Oxford University Press: Oxford, 1985; pp 175–189.
(14) Parthasarathi, V.; Beurskens, P. T.; Slot, H. J. B. *Acta Crystallogr.* **1983**, *A39*, 860–864.
(15) *TEXSAN: Single Crystal Structure Analysis Software, Version 1.6*; Molecular Structure Corporation: The Woodlands, TX, 1992.

Table 1. Crystallographic Information for $[Fe_2O(XDK)(CH_3OH)_5(H_2O)](NO_3)_2{\cdot}4H_2O$ (**1**$(NO_3)_2{\cdot}4H_2O$), *syn*-$[Fe_2O(XDK)(bpy)_2(NO_3)_2]{\cdot}3CH_3CN$ (*syn*-**4**$\cdot 3CH_3CN$), and $[Fe_2O(XDK)(1\text{-MeIm})_6](BPh_4)_2{\cdot}CHCl_3$ (**5**$(BPh_4)_2{\cdot}CHCl_3$)[a]

	1$(NO_3)_2{\cdot}4H_2O$	*syn*-**4**$\cdot 3CH_3CN$	**5**$(BPh_4)_2{\cdot}CHCl_3$
formula	$C_{37}H_{68}N_4O_{25}Fe_2$	$C_{58}H_{63}N_{11}O_{15}Fe_2$	$C_{105}H_{115}N_{14}O_9B_2Cl_3Fe_2$
fw	1080.7	1265.9	1956.8
crystal system	orthorhombic	monoclinic	triclinic
space group	*Pbcm*	$P2_1/n$	$P\bar{1}$
a, Å	11.736(3)	13.462(4)	15.133(3)
b, Å	20.635(7)	22.632(4)	23.798(3)
c, Å	22.223(7)	20.002(7)	14.468(2)
α, deg			100.74(1)
β, deg		92.92(2)	93.68(1)
γ, deg			101.26(1)
V, Å^3	5382(3)	6086(3)	4993(1)
Z	4	4	2
d_{calc}, g cm^{-3}	1.334	1.381	1.301
T, K	195	195	201
data coll range, deg	$3 \le 2\theta \le 42$	$3 \le 2\theta \le 48$	$3 \le 2\theta \le 45$
data limits	$+h,+k,+l$	$+h,+k,\pm l$	$+h,\pm k,\pm l$
no. of data collected	4852	9793	13805
p-factor[b]	0.05	0.03	0.022
R_{av}	0.020	0.040	0.033
no. of obs unique data[c]	2098	5539	7462
no. of parameters	326	775	961
data/parameter ratio	6.44	7.14	7.76
abs coeff, cm^{-1}	6.19	5.51	4.34
trans. coeff, min/max	0.887/1.000	0.945/1.000	0.934/1.000
R^d	0.068	0.056	0.056
R_w	0.089	0.066	0.059
largest shift/esd, final	0.000	0.000	0.000
largest peak, e$^-$/Å^3	0.524	0.722	0.726

[a] Data were collected on an Enraf-Nonius CAD4-F kappa geometry diffractometer using Mo Kα radiation. [b] Used in the calculation of $\sigma(F^2)$. [c] Observation criterion $I > 3\sigma(I)$. [d] $R = \sum||F_o| - |F_c||/\sum|F_o|$, $R_w = [\sum w(|F_o| - |F_c|)^2/\sum w|F_o|^2]^{1/2}$, where $w = 1/\sigma^2(F)$, as defined in Carnahan *et al.*, ref 12.

$CHCl_3$ solution at room temperature. A dichroic green-brown block (dimensions 0.3 × 0.3 × 0.4 mm) was mounted in Paratone N on the end of a quartz fiber. The data collection temperature was 201 ± 1 K. The data collection and structure solution were carried out as described above. The positions of the non-hydrogen atoms of the cation were refined with anisotropic thermal parameters. The phenyl rings of the counterions were treated as rigid bodies. The hydrogen atoms were included in calculated positions during the last cycles of the refinement. The largest peak in the final difference map was 1.0 e$^-$/Å^3, located in the vicinity of one of the BPh_4^- phenyl rings.

Physical Measurements. ^{1}H NMR spectra were collected on a Varian VXR-300 instrument. IR spectra were obtained and manipulated by using a Bio-Rad SPC3200 FTIR instrument and UV/visible spectra were recorded with a Hewlett-Packard diode array spectrophotometer. Resonance Raman data were obtained by using a Kr ion laser (excitation wavelength 406.7 nm), with an approximate incident power on the sample of 20 mW. A 0.6-m single monochromator (1200 grooves/mm grating), with an entrance slit of 300 μm, and an optical multichannel analyzer were employed in a standard backscattering configuration. A holographic Raman edge filter was used to attenuate Rayleigh scattering. Twenty scans were summed and baseline correction was applied. Stopped-flow kinetic measurements were performed with a Hi-tech Scientific SF-40 stopped flow instrument (Canterbury Stopped-Flow), interfaced to an Apple Macintosh IIfx computer using the software package Labview2. Kinetic runs were performed in triplicate, and the data were averaged prior to fitting. Data were processed and plotted using Kaleidagraph. Mössbauer spectra were collected at 100 ± 10 K using a Ranger Scientific instrument, and the experimental data were either fit to Lorentzian or Voight line shapes. All isomer shifts were referenced to iron metal at 300 K.

Results and Discussion

Syntheses. Many difficulties encountered in preparing model complexes for carboxylate-bridged dinuclear non-heme iron proteins are associated with the presence of multiple iron-containing species at equilibrium in solution.[1,16-18] Kinetically rapid substitution reactions at the metal centers compound the problem by increasing the accessibility of energetically similar coordination modes. As a consequence, the success of the commonly used "self-assembly" approach is highly sensitive to the reaction conditions. The products of dissociation or oligomerization of the dinuclear complexes are frequently obtained rather than, or in addition to, the desired dinuclear species. For example, the first syntheses of dinuclear (μ-oxo)bis(μ-carboxylato)diiron(III) models employed the facially capping tridentate ligands $[HB(pyrazolyl)_3]^-$ and 1,4,7-triazacyclononane (TACN) to preclude the formation of oligomers. Although oligomeric products were largely avoided by this tactic, stable mononuclear $[FeL_2]$ complexes were obtained in addition to the desired dinuclear species.[19,20] The structural and spectroscopic features of these initial dinuclear complexes were in excellent agreement with those of the oxidized forms of Hr and RR. These model complexes were unable to reproduce key functional features of the dinuclear iron protein cores, however, since they lack open or readily exchangeable terminal coordination sites that serve in the metalloproteins as sites for reactions with dioxygen or other exogenous ligands. When the tridentate capping ligands are replaced with analogous bidentate donors in self-assembly syntheses, oligomerization of the dinuclear core commonly occurred through formation of additional bonds to the bridging oxo group. The resulting dimer–tetramer equilibrium is shown schematically in eq 1.[16,21] In the absence of multidentate capping ligands, bridging through the terminal positions can take place, giving rise to higher nuclearity products.[22]

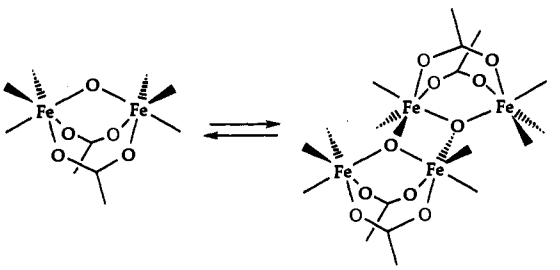

(1)

Adjustment of the reaction conditions to bias the equilibria toward the formation of dinuclear species has afforded several relevant model complexes having the formulation $[Fe_2O(O_2CR)_2B_2M_2]$, where B and M represent bidentate and monodentate ligands, respectively. The first reported example of this type of complex, $[Fe_2O(OAc)_2(bpy)_2Cl_2]$, was prepared by cleaving the tetranuclear core of $[Fe_4O_2(OAc)_7(bpy)_2]^+$ with excess bpy and chloride ion.[16] In addition, disruption of trinuclear precursors by addition of ferric ion and bidentate N-donors afforded dinuclear complexes with neutral or anionic donors as the monodentate ligands.[11] In a similar but more direct approach, a dinuclear complex was prepared by self-assembly in which the dinuclear–tetranuclear equilibrium was circumvented by an excess of the monodentate ligand.[23] Preparation of $[Fe_2O(O_2CR)_2B_2M_2]$ complexes was also accomplished by reacting carboxylic acids or

(16) Vincent, J. B.; Huffman, J. C.; Christou, G.; Li, Q.; Nanny, M. A.; Hendrickson, D. N.; Fong, R. H.; Fish, R. H. *J. Am. Chem. Soc.* **1988**, *110*, 6898–6900.
(17) Drüeke, S.; Wieghardt, K.; Nuber, B.; Weiss, J.; Fleischhauer, H.-P.; Gehring, S.; Haase, W. *J. Am. Chem. Soc.* **1989**, *111*, 8622–8631.
(18) Kurtz, D. M., Jr. *Chem. Rev.* **1990**, *90*, 585–606.
(19) Armstrong, W. H.; Spool, A.; Papaefthymiou, G. C.; Frankel, R. B.; Lippard, S. J. *J. Am. Chem. Soc.* **1984**, *106*, 3653–3667.
(20) Wieghardt, K.; Pohl, K.; Gebert, W. *Angew. Chem., Int. Ed. Eng.* **1983**, *22*, 727.
(21) Gorun, S. M.; Papaefthymiou, G. C.; Frankel, R. B.; Lippard, S. J. *J. Am. Chem. Soc.* **1987**, *109*, 3337.
(22) See, for example: Taft, K. L.; Lippard, S. J. *J. Am. Chem. Soc.* **1990**, *112*, 9629–9630.
(23) Shteinman, A. A. *Mendeleev Commun.* **1992**, 155–157.

their salts with preformed μ-oxodiiron(III) precursors,[11,24,25] and by oxidation of a diferrous precursor.[26] An interesting complex was recently described having an unsymmetrical hemerythrin-like substitution pattern.[27] In this complex, one iron bears a tridentate (Me_3TACN) capping ligand, while the other is capped by dipyridyl and a monodentate ligand L, where L = H_2O or Cl^-. Preparation of this dinuclear complex was accomplished by using mononuclear [$FeCl_3(Me_3TACN)$] and dipyridyl to disrupt the tetranuclear core of $[Fe_4O_2(OAc)_7(bpy)_2]^+$. Terminal ligand substitution was demonstrated in this system by converting the chloro to the aqua derivative following treatment with Ag^+ ion.

To date, there have been no reports of structurally characterized $[Fe_2O_2(O_2CR))_2]^{2+}$ complexes having the terminal FeM_3 substitution pattern outside of a protein environment. Spectroscopic evidence suggested the formation of such a species upon methanolysis of basic iron acetate,[22] but attempts to isolate the oxo-bridged complex resulted in condensation to give the decanuclear molecular ferric wheel, an oligomer of the [$Fe(O_2CCH_2Cl)(OCH_3)_2$] unit.[22,28]

The lack of well-characterized $[Fe_2O(O_2CR)_2(L)_6]$ complexes with exclusively monodentate terminal ligands is probably again due to multiple equilibria in solution. Since no chelate effect is operative to stabilize the binding of monodentate capping ligands such as pyridine, they will be less tightly bound and consequently less effective at inhibiting oligomerization equilibria in solution. Moreover, the pK_a values of protic solvent ligands such as methanol or water are lowered on coordination to iron(III), affording potential bridging ligands, alkoxide or hydroxide. An important tactic in preparing functional models for the carboxylate-bridged dinuclear non-heme iron proteins is therefore to gain control over the chemistry of the terminal coordination sites, since these are the sites where the biological chemistry is generally expressed. The strategy employed here to accomplish this goal has been to use a dinucleating carboxylate ligand which provides a stable, well-defined bridging environment for assembly of the dinuclear center. The ligand XDK has a cleft-like geometry originally intended to mimic the convergent arrangement of functional groups at enzyme active sites. Its preorganized binding site eliminates conformational degrees of freedom and lowers the entropic barrier to formation of metal complexes, resulting in tighter binding. Enhanced affinity for the binding of Ca^{2+} to a close relative of XDK was demonstrated previously.[7] It was therefore anticipated that binding of the $\{Fe_2O\}^{4+}$ unit to the carboxylates of XDK might impart some thermodynamic or kinetic stability to the dinuclear unit. The ligand introduces two bridging carboxylate groups in a geometry that is appropriate for binding to the (μ-oxo)diiron(III) core. Binding of this unit to the diacid sequesters the metal centers in a shallow cleft, which, due to the steric influence of the peripheral methyl groups, is quite effective at blocking the formation (eq 1) of head-to-head dimers.[29-31]

Although the rigid geometry of XDK does not precisely reproduce the disposition of the two carboxylate side chains in hemerythrin (vide infra), the ligand nevertheless binds sufficiently tightly to the oxo-bridged dinuclear Fe(III) core that assembly of the $\{Fe_2O\}^{4+}$ unit occurs rapidly on mixing 2 equiv of ferric nitrate with H_2XDK in methanol solution. The spectroscopic features of the reaction mixture clearly support this conclusion, and are similar to those observed during preparation of the molecular ferric wheel.[28] In the present case, however, the dinuclear structure of the complex persists in the solid state, so that crystallization affords multigram quantities of [$Fe_2O(XDK)(CH_3OH)_5(H_2O)](NO_3)_2$, $\mathbf{1}(NO_3)_2$, in high yield. The isolation of **1** demonstrates that XDK plays a dominant role in directing the chemistry of Fe(III) in solution. Since no capping ligands were present in the reaction mixture, we conclude that the dicarboxylate ligand is responsible for averting the formation of higher nuclearity products. Compound **1** not only represents the first structurally characterized example of a carboxylate-bridged dinuclear iron complex having exclusively monodentate ligands in the terminal sites, but the complex is of particular interest because all of the terminal ligands are exchangeable solvent molecules. This feature makes **1** valuable both as a starting material for preparing a series of closely related terminal substitution products and also because it affords an opportunity for the detailed study of terminal ligand exchange processes in solution. Both of these objectives have been met in the present work, as detailed below.

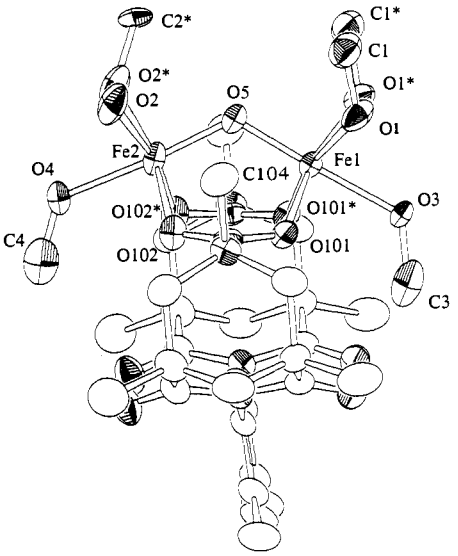

Figure 1. ORTEP plot of the $[Fe_2O(XDK)(CH_3OH)_5(H_2O)]^{2+}$ cation. Thermal ellipsoids are drawn at the 35% probability level, and hydrogen atoms are omitted for clarity. Atoms denoted by numbers with asterisks are generated by a crystallographic mirror plane. Atom O2 corresponds to the oxygen of both a water and a methanol ligand disordered across the crystallographic mirror plane that passes through Fe1–O5–Fe2.

Structure of Solid $\mathbf{1}(NO_3)_2 \cdot 4H_2O$. The X-ray structure of this complex (Figure 1, Table 2) reveals the expected bent $\{Fe_2O\}^{4+}$ core bridged by both of the carboxylate groups of XDK, with solvent ligands occupying the six terminal positions. The asymmetric unit in the crystal consists of one half of the molecule, with a mirror plane passing through Fe1–O5–Fe2. Initial attempts to refine all of the coordinated solvent molecules as methanol led to an unacceptably high thermal parameter for the carbon atom bonded to O2. The electron density was more satisfactorily accounted for with the carbon atom refined at half-occupancy, which corresponds to one CH_3OH ligand (C2*–O2*) and one H_2O ligand (O2) disordered across the mirror plane. The formula of cation **1** is therefore $[Fe_2O(XDK)(CH_3OH)_5(H_2O)]^{2+}$. The dinuclear units are linked within the crystal lattice by strong hydrogen bonds between the terminal solvent ligands and the nitrate anions, forming infinite chains. This packing arrangement results in wide channels running through the crystal structure. A significant amount of residual electron density was found in this channel, indicating that the structure is highly solvated. The most satisfactory model that we found to account

(24) Beer, R. H.; Tolman, W. B.; Bott, S. G.; Lippard, S. J. *Inorg. Chem.* **1989**, *28*, 4557–4559.
(25) Beer, R. Ph.D. Thesis, Massachusetts Institute of Technology, 1989.
(26) Tolman, W. B.; Bino, A.; Lippard, S. J. *J. Am. Chem. Soc.* **1989**, *111*, 8522–8523.
(27) Mauerer, B.; Crane, J.; Schuler, J.; Wieghardt, K.; Nuber, B. *Angew. Chem., Int. Ed. Engl.* **1993**, *32*, 289–291.
(28) Taft, K. L.; Delfs, C. D.; Papaefthymiou, G. C.; Foner, S.; Lippard, S. J. *J. Am. Chem. Soc.* **1994**, *116*, 823–832.
(29) Armstrong, W. H.; Roth, M. E.; Lippard, S. J. *J. Am. Chem. Soc.* **1987**, *109*, 6318.
(30) Gorun, S. M.; Lippard, S. J. *Inorg. Chem.* **1988**, *27*, 149.
(31) McCusker, J. K.; Vincent, J. B.; Schmitt, E. A.; Mino, M. L.; Shin, K.; Coggin, D. K.; Hagen, P. M.; Huffman, J. C.; Christou, G.; Hendrickson, D. N. *J. Am. Chem. Soc.* **1991**, *113*, 3012–3021.

Table 2. Selected Bond Distances (Å) and Angles (deg) for $1(NO_3)_2 \cdot 4H_2O$[a]

Bond Distances			
Fe···Fe	3.125(3)	Fe2–O102	2.042(7)
Fe1–O1	2.083(7)	O1–C1	1.42(1)
Fe1–O3	2.070(8)	O2–C2	1.42(2)
Fe1–O5	1.789(8)	O3–C3	1.40(2)
Fe1–O101	2.034(6)	O4–C4	1.32(3)
Fe2–O2	2.082(7)	O101–C101	1.25(1)
Fe2–O4	2.07(1)	O102–C101	1.26(1)
Fe2–O5	1.784(9)		
Bond Angles			
Fe1–O5–Fe2	122.0(5)	O2–Fe2–O2*	86.4(4)
O1–Fe1–O1*	86.1(5)	O2–Fe2–O4	83.0(3)
O1–Fe1–O3	82.9(3)	O2–Fe2–O5	94.0(3)
O1–Fe1–O101	86.2(3)	O2–Fe2–O102	87.9(3)
O1–Fe1–O5	95.4(3)	O4–Fe2–O5	175.9(4)
O3–Fe1–O5	177.7(4)	O4–Fe2–O102	86.0(3)
O3–Fe1–O101	85.6(3)	O102–Fe2–O102*	95.6(4)
O101–Fe1–O101*	99.2(4)		

[a] See Figure 1 for the atom-labeling scheme. Numbers in parentheses indicate the estimated standard deviations in the last significant digits.

for this electron density corresponds to four water molecules per formula unit. These water molecules form hydrogen-bonded chains throughout the crystal and are associated with the cations by hydrogen bonds to the imide carbonyl groups of the XDK ligand (O103, O104) and to the coordinated H_2O molecule (O2).

The structure of **1** illustrates an unusual feature in the binding mode of XDK that has been observed in all subsequently characterized Fe(III) complexes with this ligand. Whereas complexes with simple carboxylates such as acetate typically exhibit metal binding in the plane of the carboxylate group, the rigid conformation of XDK cannot accommodate such a geometry. Instead, the metal ions are situated 1.20 Å above the plane of the carboxylate groups, as illustrated in Figure 2. The magnitude of this deviation is, to our knowledge, unprecedented for a metal–carboxylate complex. Maximal overlap with the lone pairs of the sp^2-hybridized carboxylate oxygen atoms should result in the metal atoms being bound in the plane of the carboxylate oxygen and carbon atoms. A survey of dicarboxylate-bridged structures in the Cambridge Structural Database (CSD) indicates the in-plane binding geometry to be highly favored for these complexes, in accord with the results found recently for the coordination of transition metal ions to nonbridging carboxylate groups.[32] As illustrated in Figure 2, the geometric distortion can be described by the fold angle (ϕ) across the two oxygen atoms of the carboxylate group. The distance (d) of the Fe atoms from the least-squares plane of the carboxylate atoms is also a useful parameter in describing this structural feature. Values of ϕ and d for XDK derivatives are given in Table 5, from which it is clear that the binding geometry is maintained for all of the known diiron(III)–XDK structures. Such an out-of-plane binding mode might be expected to reduce overlap between the carboxylate lone pairs and the metal orbitals, and hence diminish the bond strength. This effect was observed in a complex containing the chelating dicarboxylate ligand $MPDP^{2-}$, where lengthening of the $Fe–O_{CO_2^-}$ bond occurred in association with a modest deviation (d = 0.49 Å) of the Fe atoms from the carboxylate planes.[8] The carboxylate–Fe(III) bond distances in **1** do not suggest reduced orbital overlap, however, the average $Fe–O_{COO^-}$ distance being comparable to the average value found for dicarboxylate bridged complexes in the CSD (vide infra). In addition, the spectroscopic parameters obtained for **1** and its derivatives are all within the ranges determined for other (μ-oxo)(μ-carboxylato)diiron(III) complexes, indicating that the unusual carboxylate binding mode has little influence over the bonding or electronic structure of the $\{Fe_2O\}^{4+}$ core.

Examination of the structure of **1** suggests that the carboxylate binding geometry is largely responsible for the predisposition of XDK to form di- rather than tetranuclear (eq 1)[16,21,29,30] complexes with Fe(III). Because the carboxylate groups are essentially coplanar, rather than approximately perpendicular to one another as normally observed, the Fe–O–Fe core resides in a shallow cleft that is flanked by the methyl groups (C104, Figure 1) of the Kemp's triacid moieties. The methyl groups thus hinder close approach of other molecules to the Fe–O–Fe unit. Computer modeling reveals that the binding site is sufficiently occluded that formation of oligomeric complexes by condensation of $\{Fe_2O(XDK)\}^{2+}$ units would result in highly unfavorable steric interactions between ligands. This property of XDK is analogous to the sequestering of a carboxylate-bridged dimetallic unit within the active site pocket of a protein. In complexes of unconstrained carboxylates, "in-plane" binding (Figure 2) results in the side chains being at a maximal distance from the Fe–O–Fe unit; consequently, even bulky ligands such as pivalate (R = Bu^t) do not exert a comparable steric influence over the chemistry of the $\{Fe_2O\}^{4+}$ core.

Structure of 1 in Solution. Although the X-ray crystal structure of **1**, together with molecular modeling results, strongly suggested that this complex would not oligomerize, we wished to define more rigorously its composition in solution in order facilitate interpretation of results from reactivity and kinetics studies. Comparison of the ^{57}Fe Mössbauer spectra of **1** in both the solid state and frozen methanol solution indicates, within the resolution of the technique, the presence of a single species in both cases (Figure S1, supplementary material). The spectroscopic parameters obtained from fitting to both spectra are in excellent agreement, differences in the solid state (δ = 0.55, 0.56 mm s^{-1} and ΔE_Q = 1.67, 2.06 mm s^{-1}) and frozen solution (δ = 0.56 mm s^{-1} and ΔE_Q = 1.87 mm s^{-1}) spectra presumably arising from exchange of the coordinated water ligand for a methanol upon dissolution. The broader lines of the solid state spectrum are best fit to a two-site model, having nearly equivalent values of the isomer shift (δ), but slightly different quadrupole splittings (ΔE_Q). The magnitude of ΔE_Q is influenced by the asymmetry of the iron coordination environment, and so the larger value is attributed to the Fe(III) having the H_2O ligand in the solid state. In support of the conclusion from the Mössbauer data that the complex remains intact in solution, the UV/visible spectrum of **1** also appears to arise from a single species, and the resonance Raman spectrum in methanol solution exhibits only a single ν_{sym}(Fe–O–Fe) stretching vibration at 532 cm^{-1}. We therefore conclude that, in methanol solution, the only chemistry that takes place is exchange of the coordinated water for a sixth methanol ligand, eq 2.

$$[Fe_2O(XDK)(CH_3OH)_5(H_2O)]^{2+} \xrightarrow[\text{solution}]{CH_3OH} [Fe_2O(XDK)(CH_3OH)_6]^{2+} + H_2O \quad (2)$$

Reaction of 1 with 2,2′-Dipyridyl and Solid State Structure of *syn*-$[Fe_2O(XDK)(bpy)_2(NO_3)_2]$, *syn*-4. The binding and release of exogenous ligands is of central importance to the activity of all carboxylate-bridged dinuclear non-heme iron proteins, and consequently the study of analogous reactions in model complexes has long been an important objective. Exchange reactions of both the oxo and carboxylato bridges in dinuclear models have been investigated,[17,19,33–35] the thermodynamic and kinetic aspects of the latter having been examined in detail.[17] The quantitative conversions observed in these studies were critically dependent on the resistance to oligomerization afforded by the tridentate

(32) Carrell, C. J.; Carrell, H. L.; Erlebacher, J.; Glusker, J. P. *J. Am. Chem. Soc.* **1988**, *110*, 8651–8656.
(33) Armstrong, W. H.; Lippard, S. J. *J. Am. Chem. Soc.* **1985**, *107*, 3730.
(34) Drüeke, S.; Wieghardt, K.; Nuber, B.; Weiss, J. *Inorg. Chem.* **1989**, *28*, 1414–1417.
(35) Turowski, P. N.; Armstrong, W. H.; Roth, M. E.; Lippard, S. J. *J. Am. Chem. Soc.* **1990**, *112*, 681–690.

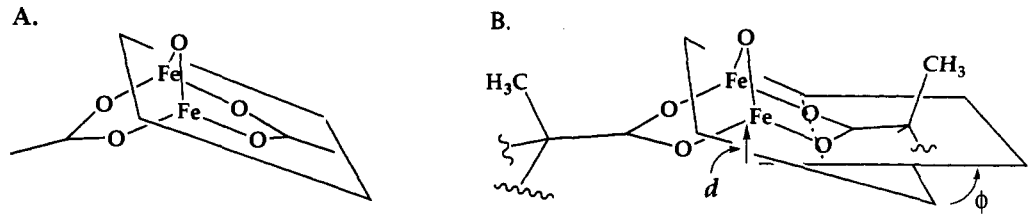

Figure 2. Comparison of typical (A) and XDK (B) carboxylate binding modes and definition of structural parameters ϕ and d used to quantitate deviation of Fe atoms from carboxylate planes.

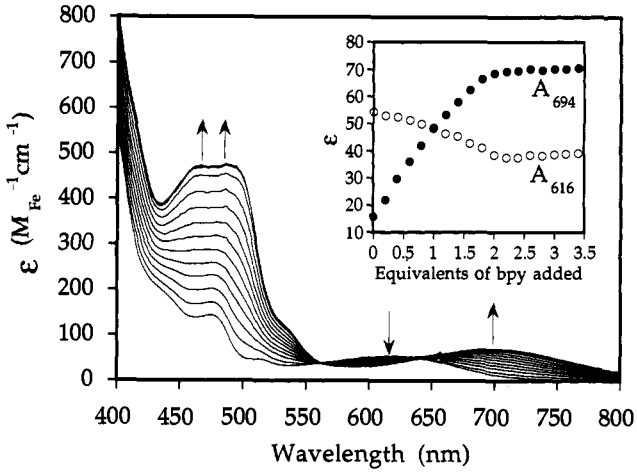

Figure 3. Titration of $[Fe_2O(XDK)(CH_3OH)_6](NO_3)_2$ with 2,2′-dipyridyl in methanol solution. Inset: Plot of absorbance at 616 nm (o) and 694 nm (●) versus number of equivalents of bpy.

capping ligands, however, and analogous work on complexes with bidentate or monodentate terminal ligands has not been previously reported. Only a few reactions involving exchange of terminal ligands in dinuclear iron complexes have been described, the most relevant being the replacement of a chloride ligand with water in the presence of silver ion.[27] The observation of catalase activity for the resulting aqua complex, which was not detected in a comparable derivative having two tridentate capping ligands, illustrates the importance of terminal ligand exchange reactions for catalysis by carboxylate-bridged dinuclear non-heme iron centers.

Since **1** has a solvent-substituted dinuclear core that resists oligomerization in solution, it provides an excellent opportunity for investigating terminal ligand exchange in a dinuclear complex. Compound **1** reacts cleanly with 2 equiv of 2,2′-dipyridyl in methanol solution to give a product having properties consistent with the terminally-capped derivative $[Fe_2O(XDK)(bpy)_2(CH_3OH)_2]^{2+}$, **2**. As shown in Figure 3, this reaction is accompanied by changes in the visible region of the spectrum consistent with coordination of N-donor ligands to iron, providing a convenient probe of the reaction. The low energy absorption band, assigned to the $^6A_1 \rightarrow [^4T_2]$($^4G$) transition, occurs at 616 nm in the spectrum of **1**, consistent with the weak ligand field provided by the solvent ligands.[8,36-38] As dipyridyl is introduced, this feature shifts to lower energy and increases slightly in intensity. The observed red shift is consistent with substitution of the stronger pyridine donor ligands into the complex. In addition, two more intense ligand field transitions, which are essentially absent in the spectrum of **1**, grow in at λ_{max} = 461 and 490 nm. As illustrated in the inset of Figure 3, the low energy bands change linearly up to 2 equiv of added dipyridyl, at which point no further change in absorbance is observed. Attempts to fit these data to an expression for the equilibrium constant corresponding to the reaction in eq 3 were unsuccessful. The absence of any curvature

$$[Fe_2O(XDK)(CH_3OH)_6]^{2+} + 2bpy \rightleftarrows [Fe_2O(XDK)(bpy)_2(CH_3OH)_2]^{2+} + 4CH_3OH \quad (3)$$

in the plot and the abrupt change in δ(A)/δ(bpy) at 2 equiv of dipyridyl indicate that K_{eq} is too large ($>10^{10}$) to be determined by this method. The reaction between **1** and bpy is thus taken to be essentially irreversible under these conditions.

Attempts to crystallize the nitrate salt of compound **2** from methanol solution afforded only **3**, in which one of the methanol ligands is replaced by a nitrate ion. An X-ray structural analysis was carried out on this product, which unequivocally established its composition. One of the nitrate counterions was severely disordered in the crystal lattice, however, and could not be modeled sufficiently well to warrant presentation of the structure here. Further recrystallization of this material from CH_2Cl_2/toluene mixtures gave the doubly nitrate substituted complex **4**. An attempt to characterize this compound by X-ray crystallography afforded only a low-angle data set ($2\theta_{max}$ 35°), since the crystal decayed rapidly with solvent loss even at −100 °C. The quality of the structure was further compromised by disordered CH_2Cl_2 solvent in the lattice. We therefore sought an alternative solvent system from which to grow crystals of **4**. Suitable material was obtained by crystallization from acetonitrile, and a structure determination was carried out. The overall molecular formula of the complex is the same as that for crystals obtained from CH_2Cl_2, with the exception of the lattice solvents. In contrast to the product obtained from CH_2Cl_2/toluene, however, the complex crystallized from acetonitrile was obtained with the unusual *syn* stereochemistry with respect to the Fe–O–Fe plane.[39] The structure, presented in Figure 4 and Table 3, has a core geometry similar to that of **1**, with the iron atoms of the Fe–O–Fe unit positioned 1.21 Å out of the carboxylate planes of XDK. The Fe–L bond distances and angles are quite similar to those found for a related complex, *anti*-$[Fe_2O(ClCH_2CO_2)_2(bpy)_2(NO_3)_2]$, **7**.[11] In particular, the complexes show similar structural features, including a lengthening of Fe–L bonds involving ligands trans to Fe–O_{br} and Fe–$O_{NO_3^-}$ compared with those involving ligands in cis positions, although the magnitude of this trans influence is smaller in **4** than in **7**. Despite the positioning of the $\{Fe_2O\}^{4+}$ unit above the plane of the carboxylate ligands, the average Fe–O_{COO^-} bond distance in **4** is statistically identical to that in **7**, again indicating that the XDK ligand is tightly bound to the (μ-oxo)diiron(III) center.

Reaction of 1 with 1-Methylimidazole and Solid State Structure of $[Fe_2O(XDK)(1\text{-MeIm})_6]^{2+}$, 5. In addition to substitution by bidentate ligands, **1** also reacts cleanly with monodentate N-donor ligands. Titration with 1-methylimidazole (1-MeIm) results in replacement of the terminal solvent ligands, giving the dinuclear complex $[Fe_2O(XDK)(1\text{-MeIm})_6]^{2+}$, **5**, as the final product. The reaction is conveniently monitored by changes in the visible spectrum (Figure 5), which resemble those for the bpy reaction described above. The lower energy $^6A_1 \rightarrow [^4T_2]$($^4G$) band shifts significantly, to 680 nm, and in this case also decreases in intensity.

(36) Reem, R. C.; McCormick, J. M.; Richardson, D. E.; Devlin, F. J.; Stephens, P. J.; Musselman, R. L.; Solomon, E. I. *J. Am. Chem. Soc.* **1989**, *111*, 4688–4704.
(37) Norman, R. E.; Holz, R. C.; Ménage, S.; O'Connor, C. J.; Zhang, J. H.; Que, L., Jr. *Inorg. Chem.* **1990**, *29*, 4629–4637.
(38) Ménage, S.; Que, L., Jr. *New J. Chem.* **1991**, *15*, 431–438.
(39) Rardin, R. L.; Tolman, W. B.; Lippard, S. J. *New J. Chem.* **1991**, *15*, 417–430.

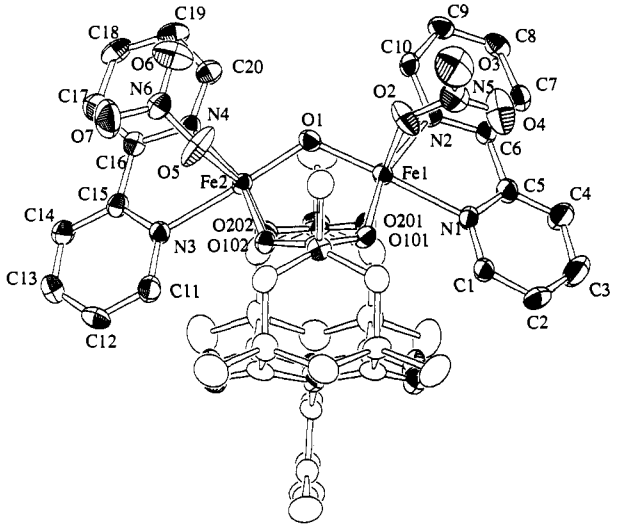

Figure 4. ORTEP plot of *syn*-$[Fe_2O(XDK)(bpy)_2(NO_3)_2]$. Thermal ellipsoids are drawn at the 40% probability level, and hydrogen atoms are omitted for clarity.

Table 3. Selected Bond Distances (Å) and Angles (deg) for *syn*-**4**·$3CH_3CN$[a]

	Bond Distances		
Fe···Fe	3.152(2)	Fe2–O1	1.795(4)
Fe1–O1	1.796(4)	Fe2–O5	2.112(5)
Fe1–O2	2.090(5)	Fe2–O102	2.032(4)
Fe1–O101	2.004(4)	Fe2–O202	2.045(4)
Fe1–O201	2.069(4)	Fe2–N3	2.178(5)
Fe1–N1	2.179(5)	Fe2–N4	2.150(5)
Fe1–N2	2.122(5)		
	Bond Angles		
Fe1–O1–Fe2	122.7(2)	O1–Fe2–O5	101.0(2)
O1–Fe1–O2	89.5(2)	O1–Fe2–O102	98.5(2)
O1–Fe1–O101	97.6(2)	O1–Fe2–O202	92.9(2)
O1–Fe1–O201	92.4(2)	O1–Fe2–N3	168.6(2)
O1–Fe1–N1	171.7(2)	O1–Fe2–N4	97.2(2)
O1–Fe1–N2	100.8(2)	O5–Fe2–O102	79.9(2)
O2–Fe1–O101	87.8(2)	O5–Fe2–O202	166.0(2)
O2–Fe1–O201	175.0(2)	O5–Fe2–N3	86.7(2)
O2–Fe1–N1	98.1(2)	O5–Fe2–N4	86.7(2)
O2–Fe1–N2	88.2(2)	O102–Fe2–O202	100.2(2)
O101–Fe1–O201	96.5(2)	O102–Fe2–N3	91.2(2)
O101–Fe1–N1	86.3(2)	O102–Fe2–N4	161.1(2)
O101–Fe1–N2	161.2(2)	O202–Fe2–N3	79.3(2)
O201–Fe1–N1	79.8(2)	O202–Fe2–N4	89.6(2)
O201–Fe1–N2	86.9(2)	N3–Fe2–N4	74.7(2)
N1–Fe1–N2	76.1(2)		

[a] See Figure 4 for the atom-labeling scheme. Numbers in parentheses indicate the estimated standard deviations in the last significant digits.

Moreover, significant increases in intensity are observed for the higher energy transitions, which shift slightly in wavelength.

In contrast to the apparently straightforward behavior of **1** when titrated with dipyridyl, the spectral changes observed in the titration with 1-MeIm indicated a somewhat more complex situation. Addition of the first 2 equiv of 1-MeIm resulted in loss of the absorption band at 616 nm, which was replaced by a broad feature in the spectrum extending from 500 to 800 nm. This behavior was independent of the concentration of **1**, and was interpreted as resulting from substitution of 1-methylimidazole into two of the terminal coordination sites on the dinuclear complex (eq 4).

$$[Fe_2O(XDK)(CH_3OH)_6]^{2+} + 2\ 1\text{-MeIm} \rightarrow [Fe_2O(XDK)(1\text{-MeIm})_2(CH_3OH)_4]^{2+} + 2CH_3OH \quad (4)$$

Substitution of the remaining four methanol ligands by addition of further equivalents of 1-MeIm (eq 5) depended on the

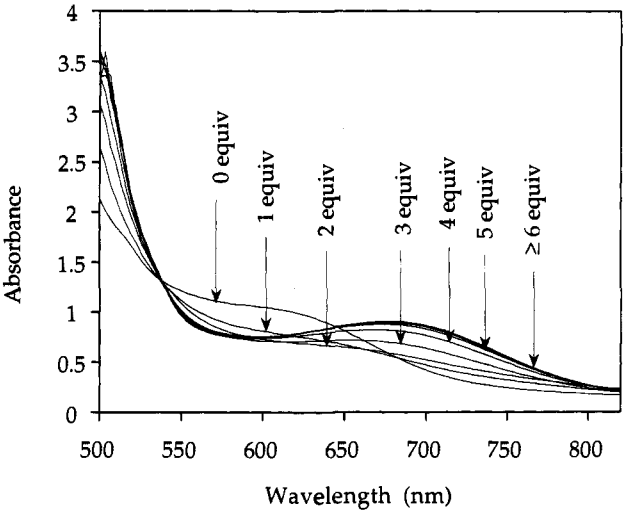

Figure 5. Changes in UV/visible spectra during titration of **1** with 1-methylimidazole in CH_3OH. Concentration of **1** = 0.13 M.

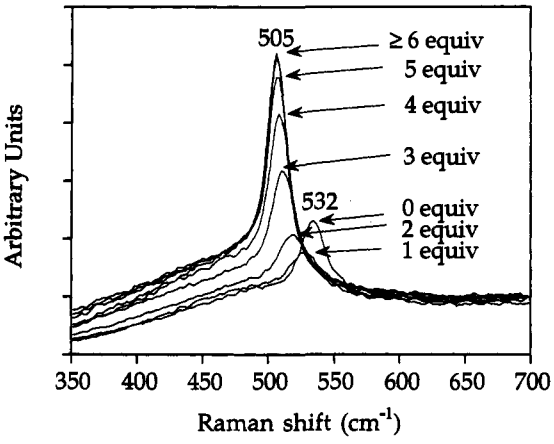

Figure 6. Resonance Raman spectral changes during titration of **1** with 1-methylimidazole in CH_3OH. Concentration of **1** = 0.10 M. Individual spectra represent a sum of 20 scans.

concentration of **1** at which the titration was performed. At

$$[Fe_2O(XDK)(1\text{-MeIm})_2(CH_3OH)_4]^{2+} + 4\ 1\text{-MeIm} \rightarrow [Fe_2O(XDK)(1\text{-MeIm})_6]^{2+} + 4CH_3OH \quad (5)$$

lower concentrations (~10 mM), the substitution reaction, monitored by the increase in A_{680}, required 30–40 equiv of 1-MeIm before it was complete. At higher concentrations (~0.1 M), however, the reaction was complete upon addition of 4 equiv of 1-MeIm. This behavior indicates that the equilibrium constants are substantially less for substitution of the four remaining solvent molecules in **1** by 1-MeIm than for the first 2 equiv. Substitution at the terminal sites of **1** therefore separates into two classes having different affinities for 1-MeIm. Since the "high affinity" and "low affinity" sites account for 2 and 4 equiv of 1-MeIm, respectively, the difference in reactivity suggests that the two positions trans to the oxo bridge might constitute the "high affinity" binding sites, with the cis sites having the lower affinity. Interestingly, in a departure from the normal behavior of (oxo)-(carboxylato)-bridged dinuclear iron(III) centers, the X-ray structure of **5**$(BPh_4)_2$ (Figure 7, Table 4) reveals that there is no lengthening of the average $Fe–N_{imidazole}$ bond trans to the $Fe–O_{br}$ unit, relative to the $Fe–N_{cis}$ distances. This result implies comparatively stronger bonding at these positions than is commonly observed. It cannot be attributed to the imidazole donor, since significant lengthening of $Fe–N_{trans}$ bonds is apparent

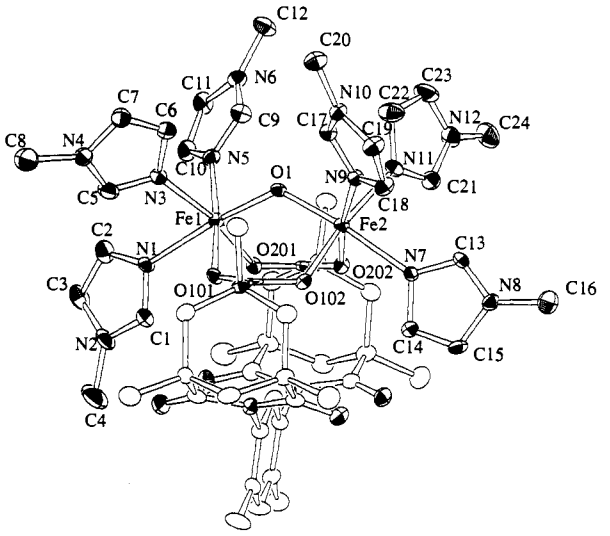

Figure 7. ORTEP plot of the $[Fe_2O(XDK)(1\text{-MeIm})_6]^{2+}$ cation. Thermal ellipsoids are drawn at the 40% probability level, and hydrogen atoms are omitted for clarity.

Table 4. Selected Bond Distances (Å) and Angles (deg) for $5(BPh)_4 \cdot CHCl_3$[a]

	Bond Distances		
Fe···Fe	3.226(1)	Fe2–O1	1.811(4)
Fe1–O1	1.814(4)	Fe2–O201	2.055(4)
Fe1–O101	2.078(4)	Fe2–O202	2.059(4)
Fe1–O201	2.050(4)	Fe2–N7	2.146(5)
Fe1–N1	2.167(5)	Fe2–N9	2.128(5)
Fe1–N3	2.155(5)	Fe2–N11	2.188(5)
Fe1–N5	2.157(5)		
	Bond Angles		
Fe1–O1–Fe2	125.7(2)	O1–Fe2–O102	91.1(2)
O1–Fe1–O101	92.9(2)	O1–Fe2–O202	95.3(2)
O1–Fe1–O201	94.0(2)	O1–Fe2–N7	173.2(2)
O1–Fe1–N1	173.9(2)	O1–Fe2–N9	90.2(2)
O1–Fe1–N3	99.7(2)	O1–Fe2–N11	97.3(2)
O1–Fe1–N5	87.9(2)	O102–Fe2–N7	82.1(2)
O101–Fe1–O201	99.8(2)	O102–Fe2–N9	89.5(2)
O101–Fe1–N1	84.6(2)	O102–Fe2–N11	170.7(2)
O101–Fe1–N3	84.9(2)	O202–Fe2–N7	85.3(2)
O101–Fe1–N5	173.6(2)	O202–Fe2–N9	169.6(2)
O201–Fe1–N1	80.9(2)	O102–Fe2–O202	99.3(2)
O201–Fe1–N3	165.3(2)	O202–Fe2–N11	84.2(2)
O201–Fe1–N5	86.4(2)	N7–Fe2–N9	90.3(2)
N1–Fe1–N3	85.7(2)	N7–Fe2–N11	89.6(2)
N1–Fe1–N5	95.2(2)	N9–Fe2–N11	86.4(2)
N3–Fe1–N5	88.6(2)		

[a] See Figure 7 for the atom-labeling scheme. Numbers in parentheses indicate the estimated standard deviations in the last significant digits.

in structures with bidentate imidazole ligands,[8,40,41] although the effect is considerably less pronounced in these cases than with pyridine or pyrazole donors. Regardless of its origin, the observation of equivalent $Fe–N_{trans}$ distances in **5** lends some support to the notion that the high affinity sites might be those situated trans to the $Fe–O_{br}$ bond. Further work is required, however, to establish this assignment definitively.

In addition to visible spectroscopy, the reaction of **1** with 1-MeIm (eqs 4 and 5) is amenable to study by resonance Raman spectroscopy, as shown in Figure 6. The spectral changes reflect differences in the energy of the ν_{sym}(Fe–O–Fe) vibration, which in turn depends on the $Fe–O_{br}–Fe$ angle.[2] Attempts to monitor the dipyridyl reaction (eq 4) by resonance Raman spectroscopy were unsuccessful, for no change in Raman shift was apparent in the spectra of the reactants and products. Subsequent crystallographic analyses of the products revealed only slight differences in the Fe–O–Fe angles of **1** and the bpy-substituted products **3**, *anti*-**4** and *syn*-**4**, so that little or no change in the Raman shift would be expected for this reaction. With 1-MeIm, however, addition of successive equivalents to a 0.1 M solution of **1** resulted in sequential changes in the spectra which terminated after addition of 6 equiv of ligand. As with the visible spectra, the Raman spectra did not display a monotonic transition between the spectra of **1** and **5**. Addition of the first equivalent of 1-MeIm shifted the maximum to lower energy, broadened the spectrum, and decreased the maximum intensity. Introduction of the second equivalent resulted in a further shift to low energy, as well as an increase in the intensity of the signal. In accord with the visible titration results, these spectral changes are consistent with substitution of the high-affinity sites on **1**, with the broadening and loss of signal intensity upon addition of the first equivalent being due to the formation of a statistical mixture of mono-, di-, and unsubstituted derivatives. Addition of the final 4 equiv of methylimidazole further diminished the vibrational frequency and considerably increased the intensity of the transition.

The resonance Raman spectral behavior of a large number of dinuclear (μ-oxo)diiron(III)-containing proteins and model complexes has been examined in detail, and the effects of the terminal substitution patterns on the energies and intensities of the spectra have been assessed.[2] From this analysis it was concluded that, whereas the presence of unsaturated N-donor ligands in the Fe coordination sphere enhances the Raman scattering intensities, the most pronounced effects result from substitution in the position trans to the oxo bridge. Since there was little change in the Raman intensity after **1** reacted with the first 2 equiv of 1-MeIm, this conclusion is inconsistent with our assignment of the high-affinity substitution sites trans to the $Fe–O_{br}$ bond. Insufficient data are currently available to resolve this issue. Attempts to characterize structurally derivatives of **1** with fewer than 6 equiv of 1-MeIm have not yet been successful.

Comparison of (μ-Oxo)diiron(III) XDK Structures with Those Related Ones in the Cambridge Structural Database. Because it was initially anticipated that the unusual binding geometry of the $\{Fe_2O(XDK)\}^{4+}$ moiety might affect the Fe–O bond strengths (and hence the bond distances) in the compounds of XDK, we have compared the metric data for the three complexes studied here with published values on related molecules. A recent statistical survey of the Cambridge Structural Database (CSD)[32] indicated that, whereas out-of-plane Fe–carboxylate binding was highly unusual, the Fe–O distances in the XDK complexes were within the normal range. Data for complexes containing carboxylate-bridged dinuclear centers were deliberately excluded from this analysis, however, rendering it invalid for comparison with the present results. We therefore carried out a limited survey of the CSD[42] to extract the relevant data for comparison with the carboxylate-bridged core of XDK.

The database was searched using standard procedures described elsewhere.[43] The structures of all complexes containing the (μ-oxo)bis(μ-carboxylato)diiron(III) motif were extracted by using the QUEST routine, which returned a total of 25 unique structures. The results of our analysis of the relevant geometric parameters, using the GSTAT routine to interrogate the statistical distributions among values, are presented in Table 5. Comparison with the average values found for the X-ray structures of **1**, *syn*-**4**, and **5** (Table 5) reveals that, with the exception of the parameters ϕ and d, which describe the binding geometry of the Fe(III) atoms with respect to the carboxylate plane (Figure 2), the values for the XDK complexes are in good agreement with those in the survey. We therefore conclude that the unusual positioning of the metal ions in the plane of the carboxylate groups of XDK

(40) Sessler, J. L.; Hugdahl, J. D.; Lynch, V.; Davis, B. *Inorg. Chem.* **1991**, *30*, 334–336.
(41) Taft, K. L. Ph.D. Thesis, Massachusetts Institute of Technology, 1993.
(42) Allen, F. H.; Kennard, O.; Taylor, R. *Acc. Chem. Res.* **1983**, *16*, 146–153.
(43) Murray-Rust, P.; Motherwell, S. *Acta Crystallogr.* **1978**, *B34*, 2518–2526.

Table 5. Comparison of X-ray Structural Data Obtained For Complexes Containing the $\{Fe_2O(XDK)_2\}^{4+}$ Core and Values for Structurally Related Complexes in the Cambridge Crystallographic Database

	XDK complexes					CSD values		
	$\mathbf{1}(NO_3)_2$	*syn*-**4**	$\mathbf{5}(BPh_4)_2$	mean[a]	std dev	mean	std dev	no. of values
Fe–O_{br}[b]	1.787	1.796	1.813	1.798	0.04	1.794	0.01	25
Fe–O_{COO}[b]	2.038	2.038	2.06	2.05	0.02	2.049	0.05	100
Fe–N_{trans}[b]		2.179	2.157	2.17	0.02	2.206	0.05	48
Fe–N_{cis}[b]		2.136	2.157	2.15	0.02	2.15	0.03	80
Fe–O_{trans}[b]	2.070			2.07		2.036	0.03	10
Fe–O_{cis}[b]	2.083	2.101		2.09	0.01	2.131	0.01	2
Fe···Fe	3.125	3.152	3.226	3.17	0.05	3.126	0.06	19
Fe–O–Fe	122.0	122.8	125.7	123.5	2.0	122.1	3.5	25
d[c]	1.21	1.21	1.20	1.20	0.07	0.246	0.16	100
ϕ[c]	37.2	37.2	36.8	37.0	2.1	7.21	4	50

[a] Average over all crystallographically independent distances in $\mathbf{1}(NO_3)_2$, *syn*-**4**, and $\mathbf{5}(BPh_4)_2$. [b] For **1**, *syn*-**4**, and **5**, values refer to averages over all such bonds in the complex. [c] See Figure 2 for definitions of these parameters.

does not substantially weaken the bonding in the $\{Fe_2O\}^{4+}$ complexes **1**, *syn*-**4**, and **5**.

Kinetics of Ligand Exchange for the Substitution of Dipyridyl for Solvent in 1. The kinetics and mechanisms of terminal ligand exchange reactions at carboxylate-bridged dinuclear centers in non-heme iron proteins are an important aspect of their reactivity. Anion binding and exchange reactions determined for metHr with N_3^-, SCN^-, F^-, Cl^-, and OH^- have revealed these reactions to be comparable in rate to substitution reactions at solvated Fe(III), with rate constants on the order of 10^2–10^3 M^{-1} s^{-1}.[44] Although kinetic data are available for bridge-exchange reactions in one model system,[17] comparison of the protein reactivities with data obtained for the more relevant terminal ligand exchange process has not been possible since no well-behaved synthetic analogues were available. Recently, kinetic studies of catalase activity in a Hr model compound were carried out, from which it was suggested that the rate-determining step may be substitution of HO_2^- for a terminal ligand in the (μ-oxo)bis(carboxylato)-diiron(III) catalyst.[27] It is therefore of interest to obtain quantitative information about the terminal ligand exchange kinetics in model systems amenable to such an investigation.

Accordingly, since ligand exchange reactions of **1** are readily monitored by changes in the visible absorption spectra (vide supra), the kinetics of the reaction of dipyridyl were measured under pseudo-first-order conditions using stopped-flow methods. Complex **1** was the limiting reagent in all experiments, and the [bpy] was allowed to vary from approximately 25- to 125-fold excess. Both the decrease in the intensity at 601 nm, corresponding to loss of **1**, and the appearance of **2**, as reflected in the increased absorbance at 461 nm, were monitored. As shown in Figure S2 (supplementary material), the kinetic traces obtained at both wavelengths give good fits to rate laws for first-order buildup and decay, respectively. A plot of $\ln(k_{obs})$ vs $\ln([bpy])$ at constant [**1**] is linear, with a slope of 1.17 ± 0.22, indicating a first-order dependence on [bpy]. Similarly, a first order dependence on [**1**] was inferred from a plot of $\ln(V_0)$ vs $\ln[\mathbf{1}]$ at constant [bpy], which had a slope of 1.13 ± 0.06. An overall second-order rate law, eq 6, therefore applies to the reaction. The first-order

$$\text{rate} = k[\mathbf{1}][\text{bpy}] \qquad (6)$$

dependence of the rate on [bpy] was confirmed by the linear fit to a plot of k_{obs} vs [bpy] (Figure 8), from which a value of (1.51 ± 0.04) × 10^3 M^{-1} s^{-1} was obtained for the second-order rate constant (k). This result is in agreement with data for terminal ligand exchange in hemerythrin.[44]

The reaction of **1** with dipyridyl is expected to occur in a stepwise manner (eq 7), with each of the two iron centers undergoing an independent substitution reaction. From the results obtained for spectroscopic titration of **1** with bpy (Figure 3), the individual steps of the reaction are effectively irreversible. One possibility

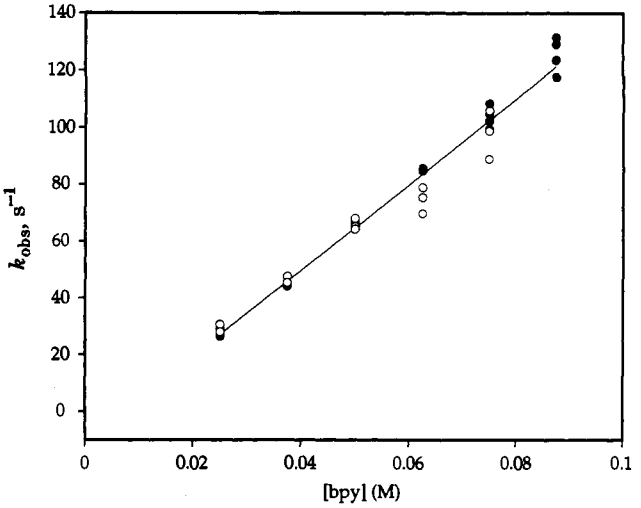

Figure 8. Plot of pseudo-first-order rate constants (k_{obs}) vs [bpy] obtained for reaction of **1** with dipyridyl in CH_3OH at a constant **1** concentration of 0.025 mM. Temperature = 296 ± 2 K. Open and closed circles indicate data obtained at 461 (appearance of **2**) and 601 nm (disappearance of **1**), respectively.

$$\mathbf{1} \xrightarrow[k_1]{\text{bpy}} \underset{\mathbf{A}}{[Fe_2O(XDK)(bpy)(CH_3OH)_4]^{2+}} \xrightarrow[k_2]{\text{bpy}} \mathbf{2} \qquad (7)$$

for the clean first-order behavior of the reaction kinetics is that k_1 and k_2 are widely different. If $k_1 \gg k_2$, one would not expect to see comparable kinetic behavior for loss of **1** and appearance of **2** unless intermediate **A** had the same spectrum as **1**. We consider this hypothesis to be unlikely, especially in view of the linear dependence of the absorption intensities on added bpy (Figure 3). Alternatively, the observed behavior may arise from the situation in which $k_2 \gg k_1$. The two Fe(III) sites in the molecule are separated by more than 3 Å, however, and no steric contact occurs between coordinated bpy ligands as revealed by the X-ray structures of **3** and **4**. It is therefore difficult to invoke a mechanism involving a dramatic rate enhancement for the second substitution process as a consequence of the first.

A likely reason for the observed first-order kinetics is the special case of two consecutive, irreversible reactions for which $k_1 = 2k_2$ and the molar extinction coefficient of the intermediate **A** is such that $\epsilon_A = 1/2(\epsilon_1 + \epsilon_2)$ (eq 7).[45] If the individual rate constants for the two steps were identical, non-first-order kinetic traces and a non-integral dependence of k_{obs} on [bpy] would result. It is reasonable to expect, however, that the two Fe(III) sites in **1** will behave independently, both kinetically and spectroscopically. In this case, k_2 would be less than k_1 by a statistical factor of 2, since **A** has only one Fe(III) site remaining for reaction with bpy.

(44) Meloon, D. R.; Wilkins, R. G. *Biochemistry* **1976**, *15*, 1284–1290.

(45) Wilkins, R. G. *Kinetics and Mechanism of Reactions of Transition Metal Complexes*, 2nd ed.; VCH: Weinheim, Germany, 1991; p 22.

Similarly, the absorption spectrum of **A** is likely to resemble that of an equimolar mixture of **1** and **2**. These conditions are precisely the ones which mask the two steps of the reaction and lead to the observation of a single first-order process.[45] In this case, the observed rate constant k corresponds to k_2, and $k_1 = 2 \times k = (3.02 \pm 0.08) \times 10^3\ M^{-1}\ s^{-1}$.

The present kinetic results support the previous observation, based on comparisons of the reactivity with simple mononuclear Fe(III) complexes such as $[Fe(H_2O)_6]^{3+}$, that substitution reactions at the active site of hemerythrin proceed with rates similar to those exhibited by small molecules in solution.[44] The carboxylate-bridged (μ-oxo)diiron(III) center neither substantially diminishes nor enhances the rate of terminal ligand substitution. It should be noted, however, that the terminal substitution rates are several orders of magnitude faster than reactions in which the bridging ligands are exchanged.[17] This information should be valuable in interpreting the reactions of biological non-heme diiron centers and their model complexes.

Summary and Conclusions

The major findings of this paper may be summarized as follows:

1. The use of a structurally constrained dicarboxylate ligand derived from studies in molecular recognition has afforded a series of oxo-bridged dinuclear Fe(III) complexes with unusual stability, including unique species with only monodentate ligands in the terminal, capping positions.

2. In contrast to complexes prepared by using simple carboxylate ligands such as acetate, these derivatives are resistant to dimerization (eq 1) and exist as dinuclear species both in solution and in the solid state.

3. Since the solvento complex remains dinuclear in solution, detailed study of the reactivity at the terminal sites of carboxylate-bridged dinuclear non-heme iron model complexes was possible. Both visible and Raman spectroscopic methods sensitively reveal features of ligand substitution by dipyridyl or 1-methylimidazole ligands.

4. The kinetics of dipyridyl ligand substitution were investigated, affording a quantitative measure of the rate constant. This work revealed that incorporation of ferric ion into the site found in several non-heme diiron carboxylate proteins does not significantly modify the intrinsic rate of terminal ligand exchange.

Acknowledgment. This work was supported by grants from the National Institute of General Medical Sciences (to S.J.L. and J.R.). We are grateful to F. M. MacDonnell and R. H. Holm for Mössbauer spectra and to A. Bakac, L. E. Pence, D. P. Goldberg, and K. L. Taft for helpful discussions. A.M. thanks the Human Frontier Science Program Organization for a fellowship and research funding.

Supplementary Material Available: Tables of complete atomic positional parameters, anisotropic temperature factors, and bond distances and angles for $\mathbf{1}(NO_3)_2 \cdot 4H_2O$, *syn*-$\mathbf{4} \cdot 3CH_3CN$, and $\mathbf{5}(BPh_4)_2 \cdot CHCl_3$ and Figures S1 and S2 displaying Mössbauer data for **1** in the solid state and in methanol solution and kinetic traces for the reaction of **1** with 2,2′-dipyridyl (49 pages). This material is contained in many libraries on microfiche, immediately follows this article in the microfilm version of the journal, and can be ordered from the ACS; see any current masthead page for ordering information.